

Comparison of HORACE and PHOTOS Algorithms for Multi-Photon Emission in the Context of the W Boson Mass Measurement

A. V. Kotwal¹ and B. Jayatilaka²

¹ *Physics Department, Duke University, Durham, NC 27708, USA. **

² *Scientific Computing Division, Fermi National Accelerator Laboratory, Batavia, IL 60510, USA.*

The W boson mass measurement is sensitive to QED radiative corrections due to virtual photon loops and real photon emission. The largest shift in the measured mass, which depends on the transverse momentum spectrum of the charged lepton from the boson decay, is caused by the emission of real photons from the final-state lepton. There are a number of calculations and codes available to model the final-state photon emission. We perform a detailed study, comparing the results from the HORACE and PHOTOS implementations of the final-state multi-photon emission in the context of a direct measurement of the W boson mass at the Tevatron. Mass fits are performed using a simulation of the CDF II detector.

PACS numbers: 12.15.-y, 12.15.Ji, 13.38.Be, 13.85.Qk, 14.70.Fm

I. INTRODUCTION

The measurement of the W boson mass (m_W) is one of the most interesting precision electroweak observables. In the standard model (SM), the mass of the W boson can be calculated with higher precision [1] than the existing measurement uncertainty [2–6], thus providing motivation for improving the statistical and systematic uncertainties on the measurement. The comparison between the theoretical prediction and the measurement provides a stringent test of the SM and constrains beyond-standard model (BSM) theories.

At hadron colliders, the mass of the W boson is extracted from inclusively-produced W bosons decaying to electrons or muons and the associated neutrinos. At the Tevatron, almost pure samples of such candidate events have been identified with backgrounds typically smaller than 1%. The momenta of the decay electrons and muons have been measured with a precision of $\sim 0.01\%$, allowing a W boson mass measurement with precision of 0.02% [6].

The calibration of the electron and muon momenta is the single most important aspect of the m_W measurement. In the approximation that the W boson undergoes a two-body decay, the distribution of the transverse momentum (p_T) [7] of the charged lepton has the characteristic Jacobian edge at half the mass of W boson. In practice, electroweak radiative corrections modify the lepton p_T spectrum, mainly due to the emission of photons from the decay lepton. If no correction were applied for this radiative process, the m_W measurement would be biased by ≈ 200 MeV [8] [20].

In the first Run II measurement [8] of the W boson mass, the WGRAD [9] and ZGRAD [10] programs were used to calculate the QED radiative correction. WGRAD and ZGRAD are exact next-to-leading order (NLO) electroweak matrix element calculations of the $q\bar{q} \rightarrow W\gamma \rightarrow l\nu\gamma$ and $q\bar{q} \rightarrow Z\gamma \rightarrow l\bar{l}\gamma$ processes, respectively. In order to increase the precision of the QED radiative correction for the W boson mass measurement, higher-order calculations were used, as implemented in the

HORACE [11–16] and PHOTOS [17–19] programs. These programs calculate the emission of multiple photons with the appropriate rates, energy and angular distributions.

PHOTOS uses the exact first-order matrix element of W and Z boson decay for the photon emission kernel. For multiphoton radiation, PHOTOS uses an iterative solution for this kernel, developed on the basis of an exact and complete phase space parametrization. This ensures not only resummation of leading-logarithm contributions of higher orders, but the infrared region of the phase space is accurately simulated as well [18, 19].

HORACE is a parton-level electroweak Monte Carlo generator for precision simulations of charged-current and neutral-current Drell-Yan processes. HORACE uses the full phase space for each radiated photon, and there is no ordering of the photons (i.e. in angle or transverse momentum) in multiphoton emission [16]. Two versions of the HORACE program are available. The OLD version [11, 12] implements a multiphoton emission QED parton shower algorithm for the simulation of final-state radiation (FSR) in the leading-logarithmic approximation, without initial-state radiation (ISR) and without interference between ISR and FSR. In this sense the OLD HORACE program is similar to the PHOTOS program, which also implements multi-photon FSR. OLD HORACE does not include full one-loop electroweak corrections, but it mimics the real radiation matrix element for the description of the photon radiation in W and Z boson decays, in the leading-logarithmic approximation [16]. There is also a NEW HORACE program [13, 14], which implements multi-photon ISR and FSR with interference, and also matches each photon to the exact matrix element calculation of one-loop electroweak corrections and single-photon emission [16].

The PHOTOS program provides a generic interface to any other event generator such that all charged leptons produced by the latter can be passed through the PHOTOS FSR algorithm. We use this feature as follows. We generate W and Z boson events for the Tevatron $p\bar{p}$ collisions at $\sqrt{s} = 1.96$ TeV, including higher-order QCD matrix elements and QCD resummation effects, but without loops or emission of electroweak bosons. We interface these events to PHOTOS such that the events from the chain contain the QED-FSR photons

*Electronic address: ashutosh.kotwal@duke.edu

added by PHOTOS. We save photons with $p_T > 0.4$ MeV and the events are processed with a detector simulation [6, 8] to make the pseudo-data and the mass-fitting templates.

In this paper we present comparisons between the distributions and the mass-fitting results obtained from the OLD HORACE and PHOTOS programs.

II. ELECTRON CHANNEL COMPARISONS

To make a direct comparisons between quantities sensitive to QED physics, we need to ensure that the underlying boson and lepton distributions are identical between OLD HORACE and PHOTOS. For this purpose we use the “Born” mode of OLD HORACE to generate Born-level $q'\bar{q} \rightarrow W \rightarrow l\nu$ and $q\bar{q} \rightarrow \gamma^*/Z \rightarrow l\bar{l}$ events, which are then processed through PHOTOS. The Born mode generates these purely $2 \rightarrow 1 \rightarrow 2$ parton processes with no radiative photons. These events are compared with events from OLD HORACE run in the QED multi-photon emission FSR mode. Both OLD HORACE and PHOTOS are run in the “exponentiation” mode. All of the events used in these comparisons have unit weights. For all generated events we make a generator-level cut on the partonic center-of-mass energy $\sqrt{s} > 40$ GeV to remove the contribution of the photon pole for neutral-current events. For consistency, we also apply this cut on the charged-current events.

In Fig. 1 we compare the distributions for photon emission rates as well as the energy and angular distributions for the $\gamma^*/Z \rightarrow e^+e^- + n\gamma$ process. For these comparisons we consider photons with energy $E_\gamma > 0.4$ MeV; photons with lower energy than this threshold are not counted and ignored in the distributions. In addition to the number n_γ of photons emitted, we find that the distributions of the following quantities are useful to compare: $\log_{10}(E_\gamma/\text{GeV})$, the fractional photon energy $y_\gamma \equiv E_\gamma/(E_\gamma + E_l)$ (where E_l is the energy of the final-state lepton) and $\Delta R(l\gamma) \equiv \sqrt{(\Delta\eta_{l\gamma})^2 + (\Delta\phi_{l\gamma})^2}$ (the $\eta - \phi$ angular separation between a photon and the final-state lepton [7]).

Figure 2 shows the photon distributions separately for low-energy and high-energy photons. These distributions show that the angular distribution is almost independent of the photon energy, allowing us to draw conclusions from the inclusive photon distributions.

The comparisons between OLD HORACE and PHOTOS show good agreement in the photon emission rates and the photon energy distributions. For the $\gamma^*/Z \rightarrow e^+e^- + n\gamma$ process, the photon angular distribution shows about 10% difference at small angles, a difference that is not correlated with photon energy. As we show in Sec. IV, this difference does not cause a relative shift in the fitted $Z \rightarrow ee$ mass between the two algorithms.

III. MUON CHANNEL COMPARISONS

We repeat the above comparisons for the muon channel. In Figs. 5 and 6 we compare the distributions for photon emis-

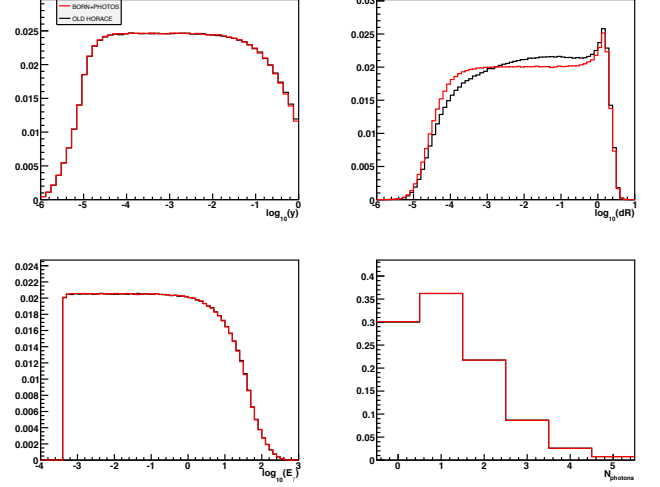


FIG. 1: Clockwise from top-left: comparisons of the distributions of $\log_{10}(y_\gamma)$, $\log_{10}(\Delta R(l\gamma))$, n_γ , and $\log_{10}(E_\gamma/\text{GeV})$ for the $\gamma^*/Z \rightarrow e^+e^- + n\gamma$ process between the “Born” mode of OLD HORACE interfaced with PHOTOS and OLD HORACE in the exponentiation mode. The smaller of the two ΔR values with respect to the two electrons is shown.

sion rates as well as the energy and angular distributions for the $\gamma^*/Z \rightarrow \mu^+\mu^- + n\gamma$ and $W^+ \rightarrow \mu^+\nu + n\gamma$ processes respectively. The rates and distributions are in good agreement between OLD HORACE and PHOTOS.

IV. MASS FITS

We quantify the impact of the small differences in photon rates and distributions between OLD HORACE and PHOTOS in terms of shifts in the fitted W boson masses. For this purpose, we propagate high-statistics OLD HORACE and PHOTOS samples through the parameterized CDF detector simulation used in the W boson mass measurement [6]. We generate templates and pseudo-data from both samples and perform the mass fits to these pseudo-data using these templates, in the same manner that templates are used to fit the collider data.

We perform fits to the distributions of transverse quantities in W boson events; the charged lepton p_T , neutrino p_T , and transverse mass m_T [21]. In the electron channel, we also perform a fit to the ratio of electron calorimeter energy to track momentum (E/p), which is used by the CDF experiment to obtain the calorimeter calibration using the electron track. In Z boson events, we fit the distributions of the Z -boson invariant-mass obtained from electron calorimeter deposition measurements (cluster mass) and from track momentum measurements of electrons and muons (track mass).

We obtain the difference between the mass fits to the HORACE pseudo-data and the PHOTOS pseudo-data which quantifies the relevant differences between the two QED codes. Tables I and II shows the differences along with their statistical uncertainties. Table I uses PHOTOS templates and is essen-

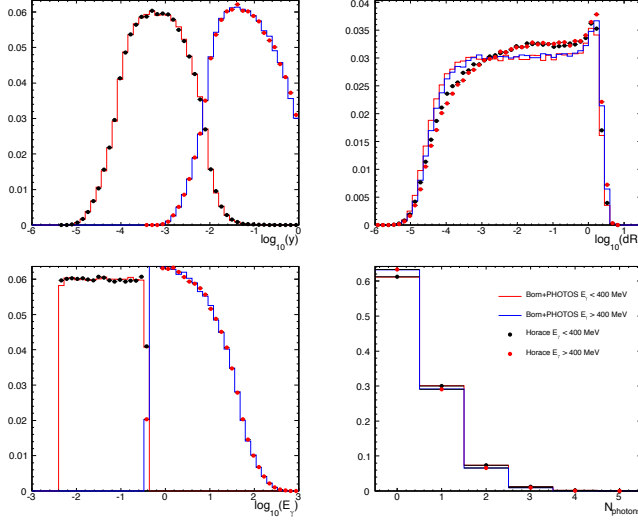


FIG. 2: Clockwise from top-left: comparisons of the distributions of $\log_{10}(y\gamma)$, $\log_{10}(\Delta R(l\gamma))$, n_γ , and $\log_{10}(E_\gamma/\text{GeV})$ for the $\gamma^*/Z \rightarrow e^+e^- + n\gamma$ process between the “Born” mode of OLD HORACE interfaced with PHOTOS and OLD HORACE in the exponentiation mode. The comparisons are shown separately for low ($E_\gamma < 400$ MeV) and high-energy ($E_\gamma > 400$ MeV) photons. The smaller of the two ΔR values with respect to the two electrons is shown.

fit type	$m_{\text{horace}} - m_{\text{photos}} \text{ (MeV)}$	
	electron	muon
W transverse mass	0.0 ± 0.6	0.0 ± 0.4
W lepton p_T	-0.4 ± 0.4	0.0 ± 0.4
W neutrino p_T	0.6 ± 0.8	1.4 ± 0.6
$W E/p$	0.4 ± 0.1	-
Z cluster mass	0.2 ± 0.4	-
Z track mass	-1.0 ± 0.6	-0.8 ± 0.3

TABLE I: Difference between HORACE and PHOTOS pseudo-data in fitted masses. The shift in the dimensionless E/p value has been multiplied by 80 GeV to convert to the equivalent shift in the fitted W -boson mass. Templates were made using PHOTOS. The statistical errors are shown. The templates and pseudo-data use 10 billion events at the generator level as the input to the detector simulation.

tially identical to Table II which uses HORACE templates. The two tables provide validation that the comparison of the two pseudo-data samples does not depend on the template choice, as long as the same templates are used for the fits being compared.

V. CONCLUSIONS

We find that the QED generators OLD HORACE and PHOTOS agree with each other in the photon rates and distribu-

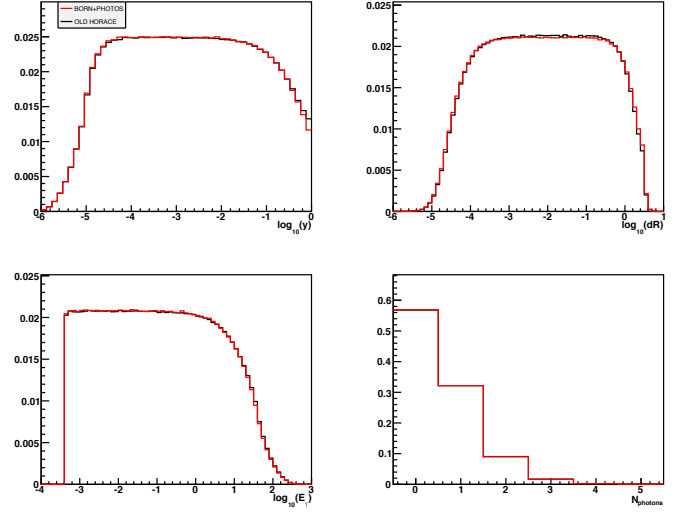


FIG. 3: Clockwise from top-left: comparisons of the distributions of $\log_{10}(y\gamma)$, $\log_{10}(\Delta R(l\gamma))$, n_γ , and $\log_{10}(E_\gamma/\text{GeV})$ for the $W^+ \rightarrow e^+ \nu + n\gamma$ process between the “Born” mode of OLD HORACE interfaced with PHOTOS and OLD HORACE in the exponentiation mode. The ΔR is computed with respect to the positron.

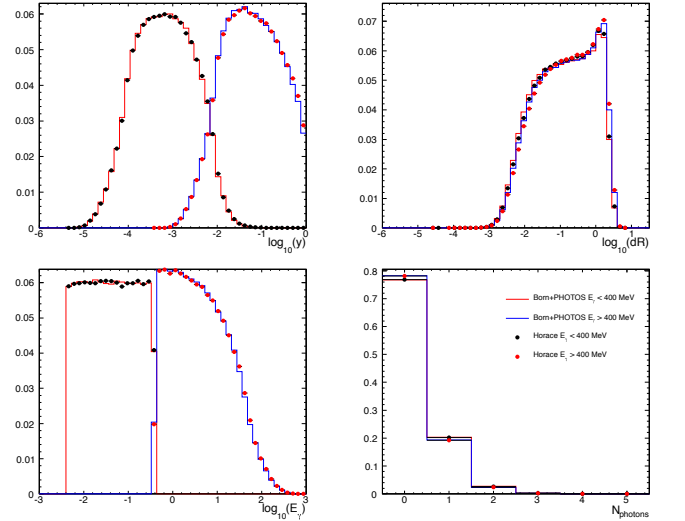


FIG. 4: Clockwise from top-left: comparisons of the distributions of $\log_{10}(y\gamma)$, $\log_{10}(\Delta R(l\gamma))$, n_γ , and $\log_{10}(E_\gamma/\text{GeV})$ for the $\gamma^*/Z \rightarrow \mu^+\mu^- + n\gamma$ process, separated into low ($E_\gamma < 400$ MeV) and high-energy ($E_\gamma > 400$ MeV) photons. The smaller of the two ΔR values with respect to the two muons is shown.

tions. The only noticeable difference is in the photon angular distribution for the $\gamma^*/Z \rightarrow e^+e^- + n\gamma$ process, at small angular separation from the nearest lepton. We quantify the comparison by computing relative W and Z -boson mass shifts, and find them to be consistent with ≈ 0.7 MeV within statistical uncertainties. We conclude that a systematic uncertainty of 0.7 MeV would account for any differences in the FSR

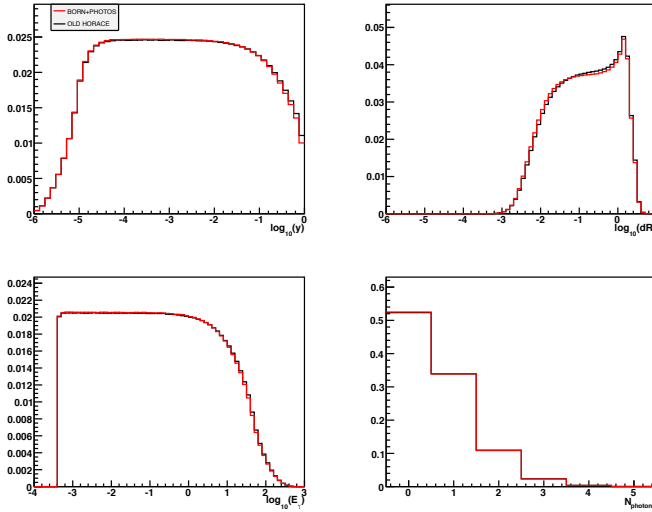


FIG. 5: Clockwise from top-left: comparisons of the distributions of $\log_{10}(y_\gamma)$, $\log_{10}(\Delta R(l\gamma))$, n_γ , and $\log_{10}(E_\gamma/\text{GeV})$ for the $\gamma^*/Z \rightarrow \mu^+\mu^- + n\gamma$ process between the “Born” mode of OLD HORACE interfaced with PHOTOS and OLD HORACE in the exponentiation mode. The smaller of the two ΔR values with respect to the two muons is shown.

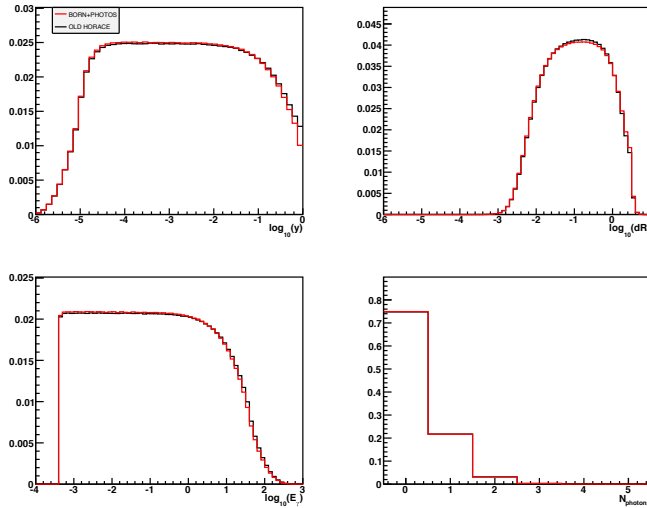


FIG. 6: Clockwise from top-left: comparisons of the distributions of $\log_{10}(y_\gamma)$, $\log_{10}(\Delta R(l\gamma))$, n_γ , and $\log_{10}(E_\gamma/\text{GeV})$ for the $W^+ \rightarrow \mu^+\nu + n\gamma$ process between the “Born” mode of OLD HORACE interfaced with PHOTOS and OLD HORACE in the exponentiation mode. The ΔR is computed with respect to the muon.

multi-photon emission between the HORACE and PHOTOS algorithms.

fit type	$m_{\text{horace}} - m_{\text{photos}} \text{ (MeV)}$	
	electron	muon
W transverse mass	0.0 ± 0.6	0.2 ± 0.4
W lepton p_T	-0.6 ± 0.4	0.0 ± 0.4
W neutrino p_T	0.6 ± 0.8	1.6 ± 0.6
$W E/p$	0.4 ± 0.1	-
Z cluster mass	0.0 ± 0.4	-
Z track mass	-1.2 ± 0.7	-0.8 ± 0.3

TABLE II: Difference between HORACE and PHOTOS pseudo-data in fitted masses. Templates were made using HORACE. The shift in the dimensionless E/p value has been multiplied by 80 GeV to convert to the equivalent shift in the fitted W -boson mass. The statistical errors are shown. The templates and pseudo-data use 10 billion events at the generator level as the input to the detector simulation.

Acknowledgments

We wish to thank Ilija Bizjak for his assistance with the HORACE program, and Zbigniew Was for providing the interface to the PHOTOS program. We wish to thank William Ashmanskas, Franco Bedeschi, Daniel Beecher, Ilija Bizjak, Kenichi Hatakeyama, Christopher Hays, Mark Lancaster, Sarah Malik, Larry Nodulman, Peter Renton, Tom Riddick, Ravi Shekhar, Melvyn Shochet, Oliver Stelzer-Chilton, Siyuan Sun, David Waters, Yu Zeng, and other colleagues in the CDF Collaboration for helpful discussions. We also thank Carlo Carloni Calame, Guido Montagna, Alessandro Vicini, Doreen Wackeroth and Zbigniew Was for discussions regarding electroweak radiative corrections. We acknowledge the support of the U.S. Department of Energy, Office of High Energy Physics and the Fermi National Accelerator Laboratory (Fermilab). The computational resources used in this study were provided by Fermilab. Fermilab is operated by Fermi Research Alliance, LLC under Contract No. DE-AC02-07CH11359 with the United States Department of Energy.

- [1] M. Baak *et al.*, *Eur. Phys. J. C* **74**, 3046 (2014).
- [2] T. Aaltonen *et al.* (CDF and D0 Collaborations), *Phys. Rev. D* **88**, 052018 (2013).
- [3] T. Aaltonen *et al.* (CDF Collaboration), *Phys. Rev. Lett.* **108**,

- 151803 (2012).
- [4] V. M. Abazov *et al.* (D0 Collaboration), *Phys. Rev. Lett.* **108**, 151804 (2012).
- [5] V. M. Abazov *et al.* (D0 Collaboration), *Phys. Rev. D* **89**,

- 012005 (2014).
- [6] T. Aaltonen *et al.* (CDF Collaboration), Phys. Rev. D **89**, 072003 (2014).
- [7] The pseudorapidity $\eta = -\log[\tan(\theta/2)]$, where θ is the polar angle with respect to the beam axis, and ϕ is the azimuthal angle about the beam axis. The transverse momentum p_T is defined as the component of the momentum perpendicular to the beam axis.
- [8] T. Aaltonen *et al.* (CDF Collaboration), Phys. Rev. D **77**, 112001 (2008).
- [9] U. Baur, S. Keller and D. Wackerth, Phys. Rev. D **59**, 013002 (1999).
- [10] U. Baur, O. Brein, W. Hollik, C. Schappacher and D. Wackerth, Phys. Rev. D **65**, 033007 (2002).
- [11] C. M. Carloni Calame, G. Montagna, O. Nicrosini and M. Trecani, Phys. Rev. D **69** (2004) 037301.
- [12] C. M. Carloni Calame, G. Montagna, O. Nicrosini and M. Trecani, JHEP **0505** (2005) 019.
- [13] C. M. Carloni Calame, G. Montagna, O. Nicrosini and A. Vicini, JHEP **0612** (2006) 016.
- [14] C. M. Carloni Calame, G. Montagna, O. Nicrosini and A. Vicini, JHEP **0710** (2007) 109.
- [15] HORACE version 3.1, <http://www2.pv.infn.it/~hepcomplex/horace.html>
- [16] C. M. Carloni Calame, G. Montagna, and A. Vicini, private communication.
- [17] E. Barberio and Z. Was, Comp. Phys. Commun. 79 (1994) 291.
- [18] Z. Was, private communication.
- [19] Andrej B. Arbuzov, Renat R. Sadykov and Zbigniew Was, Eur. Phys. J. C **73**, 2625 (2013).
- [20] Throughout this paper, we use the convention $\hbar = c = 1$.
- [21] The transverse mass is defined as $m_T = \sqrt{2p_T^\ell p_T^\nu (1 - \cos \Delta\phi)}$, where $\Delta\phi$ is the azimuthal angle between the charged lepton and neutrino momenta in the transverse plane.